Article

Revival of light signalling in the postmortem mouse and human retina

https://doi.org/10.1038/s41586-022-04709-x

Received: 9 April 2021

Accepted: 31 March 2022

Published online: 11 May 2022

Check for updates

Fatima Abbas[1], Silke Becker[1], Bryan W. Jones[1], Ludovic S. Mure[2,5,6], Satchidananda Panda[2], Anne Hanneken[3,4]✉ & Frans Vinberg[1]✉

Death is defined as the irreversible cessation of circulatory, respiratory or brain activity. Many peripheral human organs can be transplanted from deceased donors using protocols to optimize viability. However, tissues from the central nervous system rapidly lose viability after circulation ceases[1,2], impeding their potential for transplantation. The time course and mechanisms causing neuronal death and the potential for revival remain poorly defined. Here, using the retina as a model of the central nervous system, we systemically examine the kinetics of death and neuronal revival. We demonstrate the swift decline of neuronal signalling and identify conditions for reviving synchronous in vivo-like trans-synaptic transmission in postmortem mouse and human retina. We measure light-evoked responses in human macular photoreceptors in eyes removed up to 5 h after death and identify modifiable factors that drive reversible and irreversible loss of light signalling after death. Finally, we quantify the rate-limiting deactivation reaction of phototransduction, a model G protein signalling cascade, in peripheral and macular human and macaque retina. Our approach will have broad applications and impact by enabling transformative studies in the human central nervous system, raising questions about the irreversibility of neuronal cell death, and providing new avenues for visual rehabilitation.

Ischaemic events leading to the cessation of blood circulation in the central nervous system (CNS) have been traditionally thought to lead rapidly to irreversible damage of the brain. Although there may be increased electrical activity during these events, producing the sensation of bright light soon after death—the 'near-death experience'[1,3]—consciousness and brain activity are lost within a few minutes of cardiac arrest[2]. The irreversibility of neuronal 'death' has been questioned recently[4]; this involved revival of depolarization-induced spikes of individual neurons from postmortem pig brains, but not of global brain activity measured by surface biopotential (electroencephalogram). Using the retina as a model of the CNS, we tested the hypothesis that light-evoked global electrical activity originating from synchronous activity of neuronal populations can be revived after death. We first investigated the timeline and cellular mechanisms disrupting light-evoked retinal responses after circulatory collapse. We measured light-induced photoreceptor and ON bipolar cell responses (second-order interneurons receiving direct input from photoreceptors) both before and after euthanasia by cervical dislocation using in vivo electroretinography (ERG) in mice (Fig. 1a–c, Methods), a method that provides information about summed electrical activity of neurons in the retina in response to light. We identified a progressive reduction in ERG responses driven by photoreceptors and ON bipolar cells, resulting in an almost complete loss of ERG activity within approximately 5 min of death (Fig. 1c). Notably, the amplitudes of the bipolar cell responses declined with a significantly faster time constant (τ = 1.3 min; Fig. 1c, inset) than that of the photoreceptor responses (τ = 2.2 min; Fig. 1c, inset). The ON bipolar cell response appeared to be eliminated by 200 s (Fig. 1b, bottom trace), indicating that the transmission of light signals to bipolar cells is lost before the photoreceptor responses.

Knowing that in vivo light-evoked retinal responses are greatly diminished within minutes of death, we next tested whether retinal neuron activity could be revived ex vivo by restoring normal pH and oxygenation (Methods). We carried out ex vivo ERG experiments in isolated mouse retinas collected with different death-to-enucleation delays (Fig. 1d) and perfused with oxygenated (95% partial pressure of oxygen (pO_2)) physiological medium. Under these conditions, we observed a significant recovery of the photoreceptor-driven ERG a-wave and ON bipolar cell-driven ERG b-wave light responses (isolated using pharmacology and digital subtraction; Methods) when normalized to the maximal ex vivo ERG amplitudes from immediately isolated retinas (Fig. 1e, f). Unlike the rapid decline of in vivo ERG amplitudes (Fig. 1b), the ex vivo photoreceptor and ON bipolar cell light-evoked responses could be restored from 15 min up to 3 h after death. Although restored amplitudes from photoreceptor and ON bipolar cells still declined with increasing death-to-enucleation times, the ex vivo photoresponses decayed around tenfold slower than during postmortem in vivo recordings (Fig. 1f). The ON bipolar cell responses decayed about twice as rapidly as photoreceptors with increasing enucleation delay (Fig. 1f, inset). Thus, even after evoked neuronal activity has ceased following

[1]John A. Moran Eye Center, University of Utah, Salt Lake City, UT, USA. [2]Salk Institute for Biological Studies, La Jolla, CA, USA. [3]Department of Molecular Medicine, The Scripps Research Institute, La Jolla, CA, USA. [4]Retina Consultants San Diego, La Jolla, CA, USA. [5]Institute of Physiology, University of Bern, Bern, Switzerland. [6]Department of Neurology, Zentrum für Experimentelle Neurologie, Inselspital University Hospital Bern, Bern, Switzerland. ✉e-mail: ahanneke@scripps.edu; frans.vinberg@utah.edu

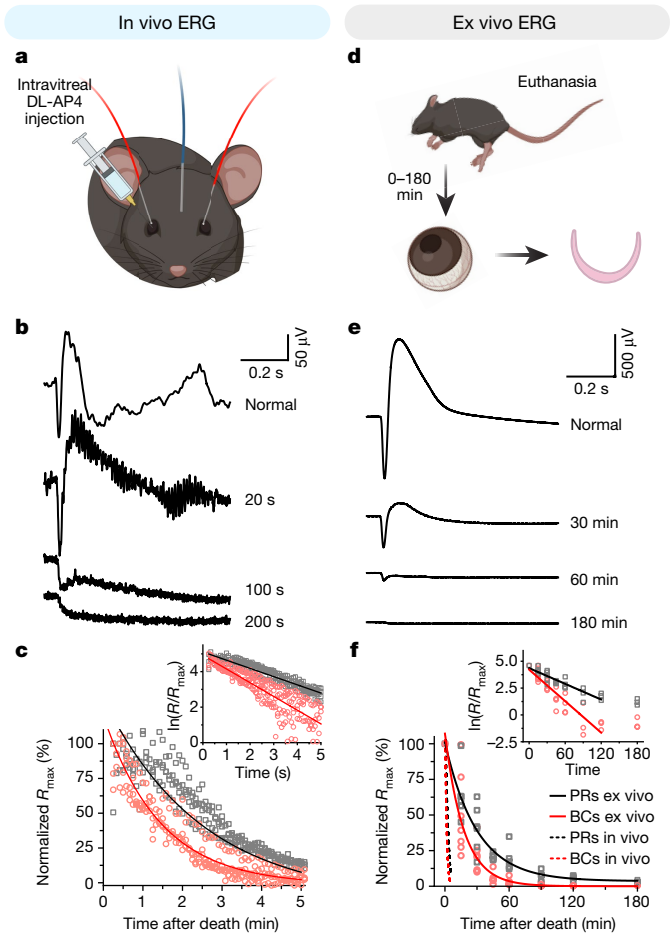

Fig. 1 | Postmortem decay and recovery of light-evoked retinal responses under in vivo and ex vivo conditions. a, Schematic of in vivo electroretinogram recordings isolating photoreceptor responses using DL-AP4 (Methods). **b**, Representative traces of in vivo ERG responses before death and between 20–200 s postmortem. **c**, Bipolar cell (hollow circles) or photoreceptor (hollow squares) light responses were detected every 5 s and normalized to the response taken before death to obtain normalized R_{max}. $n = 4$ mice. Inset, natural logarithm of normalized responses with a linear fit for photoreceptor (black line, $\tau = 2.2$ min) and bipolar cell (red line, $\tau = 1.3$ min) responses. **d**, Schematic of ex vivo ERG recording experiments (Extended Data Fig. 3, Methods). **e**, Example traces showing ex vivo restoration of light-evoked responses during recordings; responses from each retina were replicated at least three times. **f**, Ex vivo ERG responses from retinas with different death-to-enucleation delays normalized to maximal response size obtained from immediately enucleated eyes (normalized R_{max}). Inset, natural logarithm of normalized responses with linear fit up to 120 min for photoreceptor (black line, $\tau = 41$ min) and bipolar cell (red line, $\tau = 20$ min) responses. Dashed lines show fit data from **c**. For ex vivo recordings: 0 min, 8 retinas from 8 mice; 15 min, 6 retinas from 5 mice; 30 min, 5 retinas from 5 mice; 45 min, 4 retinas from 4 mice; 60 min, 4 retinas from 4 mice; 90 min, 3 retinas from 3 mice; 120 min, 3 retinas from 3 mice; 180 min, 3 retinas from 3 mice. BC, bipolar cell; PR, photoreceptor.

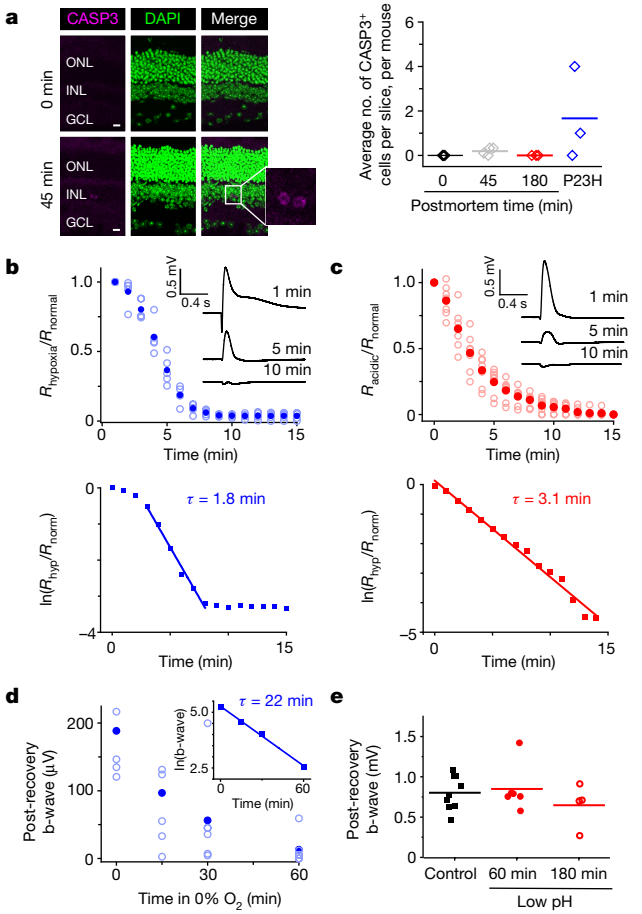

Fig. 2 | Factors affecting recovered ERG b-wave amplitudes in postmortem mouse retinas. a, Representative antibody labelling of activated caspase-3 (CASP3) in retinal sections with 0 and 45 min death-to-enucleation delay. Bottom right image shows an expanded view showing two retinal neurons with caspase-3 staining. Scale bars, 10 µm. Right, quantification of caspase-3-positive cells per slice, per mouse retina (diamonds) and the mean (horizontal lines). 0 min, 3 retinas; 45 min, 4 retinas; 180 min, 3 retinas; P23H$^{+/-}$ positive control, 3 retinas. **b**, Top, decline of b-wave amplitudes during low-oxygen perfusion normalized to R_{max} with normal perfusion ($n = 5$ individual retinas from 3 mice represented as hollow circles; solid circles indicate mean); inset, representative responses from a single retina at different time points during hypoxia. Bottom, linear fit to plotted natural log of hypoxic b-waves. Decay rate (τ) is indicated. **c**, Top, decay of b-wave amplitudes measured during perfusion in low pH (6.8) Ames perfusion normalized to amplitude in physiological pH (7.4) Ames perfusion ($n = 7$ individual retinas plotted as hollow circles; solid circles indicate the mean). Inset, representative responses from a single retina at different time points during low pH perfusion. Bottom, linear fit of the natural log of the normalized b-wave responses. Decay rate is indicated. **d**, Decline of ON bipolar responses after incubation in low oxygen for 0–60 min (0–30 min, $n = 6$; 60 min, $n = 7$). Inset, natural log of b-wave responses versus time. Decay rate is indicated. **e**, Recovery of b-wave amplitudes after incubation in low pH Ames for 60–180 min (control, $n = 9$; 60 min, $n = 6$; 180 min, $n = 4$). n refers to both number of retinas and number of mice, unless otherwise indicated.

death, light-evoked photoreceptor responses can be revived with the restoration of perfusion ex vivo.

Changes affecting loss of light signals

Our results demonstrate a substantial but incomplete recovery of the amplitudes of mouse photoreceptor and ON bipolar cell light responses after extended death-to-enucleation delays (Fig. 1f). To determine whether the partial loss of response amplitude is owing to apoptosis in photoreceptor and ON bipolar cells, we assessed activated caspase-3 protein in sections from eyes with different death-to-enucleation delays. Only a small fraction of cells in retinas from wild-type mice enucleated at 0, 45, or 180 min after death were positive for activated caspase-3, whereas activated-caspase-3 could be detected in positive control retinas experiencing photoreceptor degeneration (21-day-old *Rho*$^{P23H+/-}$ (hereafter P23H$^{+/-}$) mice; Fig. 2a, Methods). This shows that apoptotic cell death has not been induced in these neurons and is not

responsible for the incomplete recovery of responses during the 3 h postmortem interval, suggesting that photoreceptor and bipolar cell function could be fully recovered.

Since the loss of circulation and respiratory function after death leads to a fall in oxygen concentration and pH[5,6], we hypothesized that prolonged hypoxia and/or acidification of retinal tissue reduces the light-evoked responses that were recovered ex vivo and limits signal transmission from photoreceptors to ON bipolar cells. We used the light-evoked ERG b-wave, driven mainly by ON bipolar cell activity, as a marker for retinal viability and quantified the separate contributions of hypoxia and acidosis to its loss (Methods). We measured light responses from retinas isolated from eyes enucleated immediately after death ($t = 0$) and perfused under low pO_2 or increased H^+. We found that reducing pO_2 from 80% to around 5% at the retina (Methods) did not compromise phototransduction or transmission of light signals. However, reducing oxygen to below 2.5%, the expected concentration in vivo[7], rapidly compromised light signalling in the retina (Fig. 2b, top), with a time course similar to the decay observed in vivo (Fig. 1c). The second phase of the logarithmic amplitude data, in which most of the decay occurs, results in an exponential decay time constant of 1.8 min (Fig. 2b, bottom), marginally slower than the 1.3 min observed in vivo for mouse ON bipolar cell responses (Fig. 1c). These results suggest that postmortem hypoxia contributes substantially to the rapid loss of retinal light signals after death shown in Fig. 1a–c.

Next, we measured the kinetics of loss of light-evoked b-wave amplitudes under low pH conditions. In postmortem eyes, the pH declines[6] to approximately 6.8; we therefore compared b-wave responses under physiological (7.4) and low (6.8) pH by adjusting the bicarbonate concentration of the perfusion medium while maintaining 5% CO_2. Low pH exposure led to a decay of b-wave amplitudes with a time constant of 3.1 min (Fig. 2c). In vivo light responses decayed slightly faster after death (Fig. 1a–c) than under ex vivo low O_2 (Fig. 2b, top) or low pH (Fig. 2c, top) conditions. This could be owing to more severe hypoxia or acidosis compared with our ex vivo modifications or to the additive effects of multiple biochemical changes in the eye after death. Nonetheless, on the basis of our in vivo results, hypoxia and/or acidosis are dominant factors in the loss of retinal light signalling after death.

We next tested whether extended exposure to postmortem low pO_2 or low pH irreversibly limits full recovery of b-wave response amplitudes. We incubated mouse eyes for up to 180 min in low pO_2 (0%) or low pH (6.8) conditions and measured the amplitudes of ex vivo ERG b-wave responses from their retinas under standard conditions. We found that prolonged hypoxic incubation irreversibly reduces b-wave amplitudes even after a recovery period under normal perfusion conditions (Fig. 2d). The recovered b-wave amplitudes decayed as a function of hypoxia exposure time according to a single exponential function ($\tau = 22$ min; Fig. 2d, inset), close to the decay rate in ex vivo ERG enucleation delay experiments ($\tau = 20$ min; Fig. 1f, inset (red)). Together these data suggest that prolonged exposure to hypoxia either before or after enucleation limits the full recovery of retinal function. By contrast, b-waves driven by ON bipolar cells could be fully restored by transferring retinas to normal pH even after bipolar cell function had ceased under low pH conditions (Fig. 2c, top, e). These findings contrast with the effects of low pO_2 and indicate that postmortem hypoxia rather than acidosis is the rate-limiting factor causing incomplete restoration of retinal light responses after extended death to enucleation times.

During postmortem anoxia, the concentrations of many metabolites in blood and tissues change[6,8]. These changes could alter the concentrations of small signalling molecules such as glutamate or GABA (γ-aminobutyric acid), potentially explaining the compromised light signal transmission observed in postmortem retinal tissues. Here we investigated whether changes in these signalling molecules in the retina are consistent with the rapid loss of light signal transmission from photoreceptors to ON bipolar cells after death. Using computational molecular phenotyping (CMP) (Methods) we quantified changes in the metabolic profiles of photoreceptors (outer segments and somata), bipolar cells and Müller cells. After 45 min postmortem, we observed decreased taurine concentrations in all three cell types, particularly in photoreceptors (Extended Data Fig. 1a, b). Taurine has several roles in the CNS, including regulation of calcium transport and homeostasis, as well as protection against glutamate-induced calcium excitotoxicity[9]. Both glutamine and glutamate were reduced in all cells at 45 min postmortem (Extended Data Fig. 1b). The loss of both glutamate and glutamine—the neurotransmitter required for transmission of photoreceptor potentials to bipolar cells and a key metabolite involved in its production—could contribute to the rapid loss of ON bipolar cell light responses after death.

To understand whether the biochemical reactions of phototransduction are affected by death-to-enucleation delay, we used ex vivo ERG data from mice to quantify several parameters of the phototransduction cascade. We found no significant differences in the light sensitivity of photoreceptors with increasing death-to-enucleation delay, indicating the fraction of light-sensitive channels closed by a photon remains unchanged (Extended Data Fig. 2a–d). However, there was a trend towards smaller gain of phototransduction activation reactions (Extended Data Fig. 2e) and lengthening of dim flash time to peak (t_p) and integration time (T_i) after 90 min postmortem (Extended Data Fig. 2f, g), suggesting that the activation and inactivation reaction kinetics of phototransduction cannot be fully restored when more than 90 min have elapsed after death using the current protocols. However, these changes in the gain and kinetics of phototransduction are modest when compared with the significant and gradual decay of the maximal photoresponse (R_{max}) after death (Fig. 1f).

Restoration of macular phototransduction

We have demonstrated that limited recovery of photoreceptor and ON bipolar cell light responses is possible several hours after death in the rod-dominated retina of the nocturnal mouse. However, the human retina is structurally distinct, and contains a central macula and fovea with a high cone density and a higher metabolic rate[10]. Therefore, restoring light signals in human macular photoreceptors after death is expected to be more challenging. A recent study showed that ischaemia induces transcriptomic changes in human peripheral photoreceptors and other retinal cells within as little as 3 h postmortem[11]. This may explain in part why only a few studies have reported ex vivo human photoreceptor light responses from retina samples obtained from live patients[12–14] or from donor eyes removed several hours postmortem[15–18]. To our knowledge, light responses from human macular photoreceptors have not previously been reported and the time course for revival of human photoreceptor light responses has not been quantified, both of which are key impediments to advancing our understanding of human vision, vision disorders and visual rehabilitation.

We optimized our specimen holder to isolate electrical signals from a well-defined central sampling area (0.5–2 mm in diameter; Extended Data Fig. 3; see also refs. [19,20]) to record high signal-to-noise ratio light responses compared with pioneering ex vivo ERG studies (for example, in refs. [21,22]). We progressed to recovering macular photoreceptor light responses in explants from donor human eyes recovered within 2–5 h postmortem. Using this approach, we recorded ex vivo cone photoreceptor light responses from macula of human eyes enucleated up to 5 h postmortem (Extended Data Fig. 4b). Under these conditions, we did not observe ERG b-waves in any macula samples ($n = 17$), but we did record ERG b-waves in a peripheral sample from one donor (Extended Data Fig. 5e, f). To overcome these limitations, we conducted additional experiments with eyes obtained after cardiac death with death-to-enucleation delays of approximately 45 min to 2 h (Extended Data Fig. 4, filled triangles). We observed strong

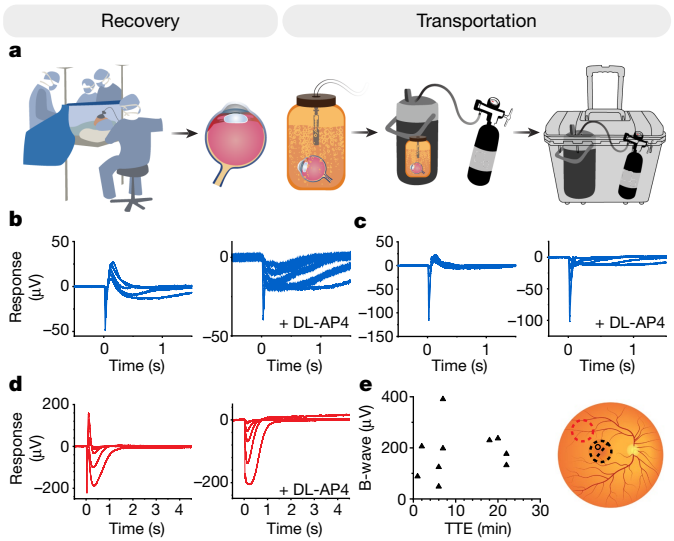

Fig. 3 | ERG b-wave is preserved in freshly obtained retinas from human donors after brain death. a, Schematic of process for maintaining optimal function of retinas from donors after brain and cardiac death (Methods). **b**, **c**, Example ex vivo ERG recordings from the parafoveal and perifoveal (**b**) and foveal (**c**) regions of the retina with responses in the absence (left) and presence (right) of DL-AP4. **d**, The peripheral retina shows larger response amplitudes both in the absence (left) and presence (right) of DL-AP4. **e**, Left, maximal b-wave amplitude measured from peripheral retina of organ donors after brain death plotted against the delay to enucleation (10 pieces of 8 eyes from 5 donors). Right, schematic showing approximate locations of peripheral (red) and macular (black) samples.

photoreceptor response amplitudes that were not statistically different from those measured from freshly enucleated macaque eyes (Extended Data Fig. 4a, c). However, we were still unable to restore robust b-waves even when we minimized the postmortem hypoxic period during transportation to the laboratory with oxygenation (Fig. 3a). Our data show a fast decay of rod and cone ON bipolar cell responses in mice (Fig. 1f, Extended Data Fig. 6a) and an absence of ON bipolar cell light responses in human macular cones from donor eyes enucleated >45 min after death (Extended Data Fig. 4b). These results are consistent with previous studies showing that the b-wave is vulnerable to retinal ischaemia[22–25]. Since robust evoked responses can still be observed from individual ganglion cells around 45 min after death[26,27] or under conditions in which the b-waves are absent[24], it is possible that the revival of the b-wave is limited by factors causing an incomplete restoration of synchronous activity from multiple ON bipolar cells, a requirement for a robust generation of an extracellular biopotential[4].

Using human donor eyes introduces several uncontrolled variables, including death-to-enucleation delay, cause of death, co-morbidities, retinal disease and donor age. First, we performed linear fit to the $\ln(R_{max})$ data plotted against enucleation delay and performed Pearson's correlation analysis (Extended Data Fig. 4c, inset), showing a significant negative correlation between $\ln(R_{max})$ and enucleation delay, with an exponential time constant of 74 min, almost double that determined for mouse photoreceptors (Fig. 1e, f). This difference could be the result of the higher cone density in the humans versus higher rod density in mouse, or other species differences. To test this, we determined how death-to-enucleation delay affects cone photoreceptor responses in mice whose rods do not respond to light (*Gnat1*$^{-/-}$; Methods). The time constant of decay was longer for mouse cones than for mouse rods (53 min versus 41 min; Fig. 1f, inset, Extended Data Fig. 6a). Notably, the postmortem decay of mouse cones was not statistically different from that of human macular cones. These data suggest that cone function is more resistant to enucleation delay than rod function, which was not expected, since cones have higher energy demands than rods. Further research is required to fully understand the contributions of species, photoreceptor type and retinal location to the kinetics of postmortem decay of light responses. Next, we examined the association between cause of death or donor age and restoration of human macular cone R_{max} after death to identify parameters that would be predictive of optimal viability in future human grafts. Comparing R_{max} from the three most common causes of death indicates that sepsis and acute cardiac events produced a much lower R_{max} than stroke (Extended Data Fig. 5d). Of note, the only donor in this study whose retina samples were able to generate b-waves (in peripheral retina) died of stroke (Extended Data Fig. 5e, f). Finally, we found a positive correlation between donor age and R_{max} (Extended Data Fig. 5c). It is possible that the larger responses from older donors could be a result of our exclusion criteria selecting donors with no ocular disease history, or because the liquefaction of the vitreous in older patients promotes better retinal access to oxygen and nutrients. Older eyes may also have a lower metabolic rate or premortem exposure to hypoxic pre-conditioning events that are known to promote postmortem viability of other organs (reviewed in ref. [28]). However, there are too many compounding factors to draw precise conclusions about the roles of age and cause of death or their underlying mechanisms. Understanding these factors will enable a more consistent revival of intact light signalling in human retina samples—crucial future work. Our data suggest that increased donor age does not negatively affect physiological recordings and that cause of death is an important consideration when setting the donor criteria.

Synaptic signalling in the human retina

The recovery of light-evoked macular photoreceptor responses from human eyes enucleated up to 5 h postmortem unlocks the potential for using these tissues to understand human photoreceptor physiology and supports the potential for future transplantation. Previous studies have recorded light responses from ganglion cells in the peripheral retina of human eyes with tumours[29–31] or from donors, enucleated immediately[11] or around 45 min to several hours after death[26,27]. However, in our experiments we were unable to consistently restore b-waves. We set out to establish the criteria and protocols to obtain viable human retina explants with intact light signalling from photoreceptors to bipolar cells.

Our data implicate pre- or postmortem hypoxia as the primary cause of irreversible b-wave loss. To address this, we used eyes from organ donors with a postmortem hypoxic time under 20 min (Fig. 3a). We were able to consistently record b-waves, specifically from peripheral retina samples with death-to-enucleation delays between 1 and 20 min (in 10 retina pieces from 8 eyes from 5 donors; Fig. 3d, e). DL-2-Amino-4-phosphonobutyric acid (DL-AP4), a blocker of metabotropic glutamate receptors expressed in ON but not in OFF bipolar cells, abolished this positive inflection both in the macular and peripheral samples, demonstrating its generation via light signal transmission from photoreceptors to ON bipolar cells (Fig. 3b–d). Using blockers of ionotropic glutamate receptors and/or longer steps of light could enable investigation of OFF bipolar cell responses and their contribution to the ERG signal in different geographical regions of the human retina[32,33], an interesting future application of our approach.

The strength of the b-waves as quantified by maximum amplitude does not correlate with enucleation delays of less than 20 min (Fig. 3e). This suggests that enucleation less than 20 min postmortem is sufficient for functional viability of the retina, with the variability in the level of retinal function probably being related to potential hypoxic events before death. Since we did not observe b-waves from donors with 45 min to 5 h of enucleation delay (Extended Data Fig. 4), the most common explanation for the irreversible loss of b-waves is extended

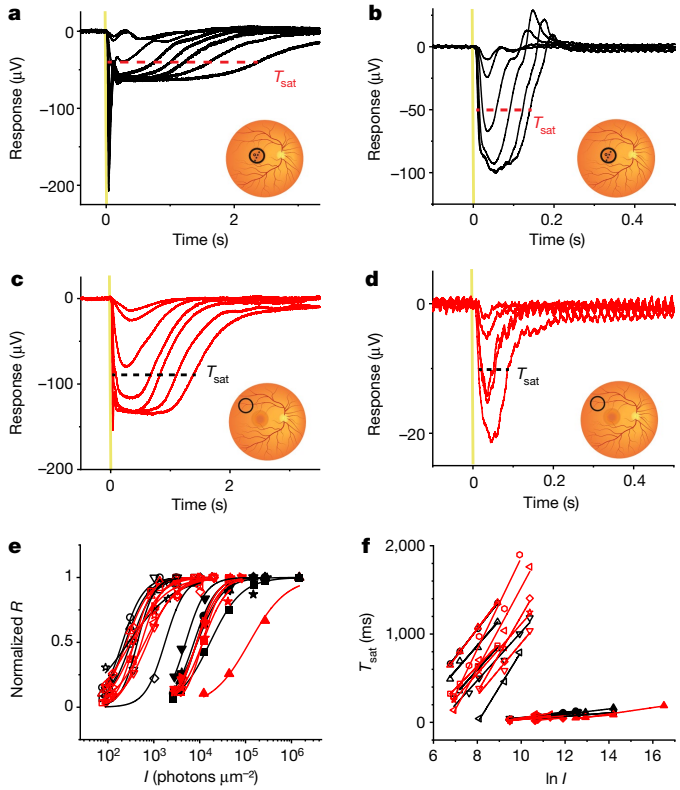

Fig. 4 | Comparison of phototransduction in rods and cones of the macula and periphery of freshly obtained retinas from human donors. a–d, Examples responses to different light intensities of photoreceptors from freshly enucleated human eyes. Insets show approximate locations from which samples were taken. **a**, Macular photoreceptors. **b**, Macular cones. **c**, Peripheral rods. **d**, Peripheral cones. Dashed red line indicates the amplitude at which the recovery from saturated response (T_{sat}) is measured (70% for rods and 50% for cones). **e**, Response amplitudes (R) normalized to R_{max} from rods and cones, plotted against flash intensity. Lines show fit to Hill function (Methods, equation (3)), used to calculate the photoreceptor sensitivity ($I_{½}$; values presented in Supplementary Table 2). Number of samples: macular rods, 6; macular cones, 6; peripheral rods, 7; peripheral cones, 7. **f**, Recovery times of macular and peripheral photoreceptors from saturation to the threshold level (T_{sat}) at different light intensities plotted against the natural log of flash intensity. Lines show linear fit (Methods, equation (4)) to determine the slope (τ_D), equivalent to the rate constant of the slowest phototransduction reaction (values presented in Supplementary Table 1). Number of samples: macular rods, 5; macular cones, 6; peripheral rods, 7; peripheral cones, 7, taken from 4 eyes of 2 donors.

time of postmortem hypoxia (more than 45 min). In some rare cases, unknown factors enable the revival of the b-wave even after 5 h of postmortem anoxia (Extended Data Fig. 5e, and fig. 2a in ref. [16]), perhaps by contributing to increased hypoxia resistance. It is of some interest that pharmacologically isolated photoreceptor responses in macular samples from organ donors (Fig. 3b, c)—but not from research donors (Extended Data Fig. 4b)—had a slower rod component, observed as a plateau phase with brighter light flashes. This could be related to rods being more susceptible to longer postmortem light exposure and/or enucleation delay, as our mouse data indicated.

Deactivation of phototransduction in human

The macaque has been used as a model to study human retinal physiology. Previous studies have highlighted differences as well as similarities in light signalling and gene expression between human and macaque retina[12,18,30,34–36], indicating that this model is not without its limitations. Divergence is also expected specifically in the context of aging and disease[37]. We used our approach to quantify the slowest deactivation reaction of human phototransduction in macular rods and cones, which is expected to rate-limit the speed of human vision[38] and is a critical gap in our knowledge of human retinal physiology. We analysed light responses in human organ donor eyes of photoreceptors isolated using DL-AP4. Responses from a representative sample in a human parafoveal macula had a large initial peak reaching around 200 μV as well also a slower plateau phase around 60 μV (Fig. 4a). To determine the rate constant of the slowest reaction ($1/\tau_D$) in the phototransduction cascade, we used a method introduced by Pepperberg et al. [39] (Fig. 4, Methods). Using this analysis, we found that τ_D—that is, the lifetime of the longest-living photoproduct—in human macular cones is 24 ms (Fig. 4b, f, Extended Data Fig. 7, Supplementary Table 1). This is considerably shorter than the lifetime of active rhodopsin or phosphodiesterase in mouse rods[40,41]. Overall, our results suggest that deactivation of phosphodiesterases and visual pigments in human macular cones is markedly faster compared with those in rods, contributing substantially to lower light sensitivity and faster kinetics of human cone-mediated high-acuity colour vision compared with scotopic rod-mediated vision. Visual disorders such as age-related macular degeneration affect primarily peri- and parafoveal rod photoreceptors, which seem to be most vulnerable to age-related deterioration[42,43]. Studying the physiology of the human rods near the fovea has presented difficulties, since they are outnumbered by cones in this area. However, using our approach, we could determine the rod saturation times in the macula, as shown in Fig. 4a. We found that the τ_D of human macular rods was more than tenfold longer than that of macular cones. We did not observe any differences between macular rods and peripheral rods from healthy donors (Fig. 4a, c, f, Supplementary Table 1).

We next compared light responses between human and macaque macular and peripheral cones. Amplitudes of the cone response were approximately five times smaller in the human peripheral samples than in the macular samples (Fig. 4b, d). However, the sensitivity was not significantly different between macular and peripheral cones (Fig. 4e, black and red filled symbols, Supplementary Table 2). Similarly, we did not find a significant difference in τ_D between macular and peripheral cones (Fig. 4f, black and red filled symbols, Supplementary Table 1). Since a recent study found slower activation kinetics and longer time to peak of the foveal cone responses in macaques[44], we compared dim flash responses of the human macular and peripheral cones (Extended Data Fig. 8a, b). We did not find a difference in time-to-peak or kinetics of the initial rising phase between peripheral and macular cones. However, dim flash sensitivity was larger in macular than in peripheral cones (Extended Data Fig. 8b). Finally, τ_D was 15 and 20 ms in macaque macular and peripheral cones, respectively (Extended Data Fig. 9). These are similar to, but slightly faster than, that of human cones in our recordings. Overall, these findings are consistent with an in vivo study that analysed averaged cone responses across the human retina[45] (not specifically in the macula). It is possible that we could not distinguish small differences in kinetics between macular and peripheral human cones in our dataset, which was recorded mainly from the para- and peri-foveal areas of the macula. We also did not use blockers of ionotropic glutamate receptors and thus a component from OFF bipolar cells could, in principle, contribute to the shape of our ex vivo ERG cone responses[32]. However, this would not affect determination of τ_D, a parameter that we focused on in this study. It will be interesting to study the detailed physiology of foveal, parafoveal, perifoveal and peripheral human photoreceptors, and how they are affected in aging or disease, something that currently cannot be done using in vivo ERG or in macaques.

In summary, we have used the retina as a model for the central nervous system to systemically study the kinetics of its death and neuronal recovery from mouse and human retina. We produced ex vivo recordings of human cones with topographical specificity. We performed

this study using an enabling approach for reviving in vivo-like evoked electrical signalling, which could be applied to other neuronal tissues in the CNS. We have identified key modifiable factors—postmortem hypoxia and acidosis—that could extend the time window for recovery of trans-synaptic neuronal transmission in the CNS, thereby raising questions about the irreversible nature of neuronal death.

The methods and criteria described here could have global applications in brain and vision science research. First, ex vivo recordings of viable human retinal explants would cause a paradigm shift in the study of basic visual physiology, as well as the causes and treatments of ocular disease, similar to how the development of histochemical techniques transformed biomedical research and diagnosis of human disease. Functional human macular and peripheral retina explants provide a new platform for studying the effects of drugs on human rod and cone phototransduction, a prototypical G-protein-coupled-receptor signalling cascade, and in some cases on synaptic transmission, and how high-acuity colour vision is affected in aging and in disease, questions that have not been easy to study outside of nonhuman primate models. To demonstrate this, we have determined the kinetics of the rate-limiting phototransduction deactivation reaction in peripheral and macular human photoreceptors and pharmacologically blocked synaptic transmission between photoreceptors and ON bipolar cells in human peripheral and central retina. Notably, this research can be done without causing any harm to animals (including humans) and is more economical than nonhuman primate research. Consequently, this approach will be easier to explain to the general public and is expected to facilitate the generation of new knowledge about human neurons and neurodegenerative diseases, a major challenge in the aging society of developed countries.

Since the retina is part of the CNS, our restoration of the b-wave in this study raises the question of whether brain death, as it is currently defined, is truly irreversible. One definition of brain death requires the synchronous activation of various neurons to give rise to prototypical extracellular biopotentials (for example, the electroencephalogram gamma wave), which was not recovered in postmortem pig brains in a recent study[4]. This could be partially explained by the cocktail of antagonists that was included in the BEx perfusion media in that study[4]. Here we revived trans-synaptic signalling in retina of enucleated eyes from both mouse and human, and restored the ex vivo ERG signal—an extracellular biopotential—resembling those recorded from living subjects. We did not demonstrate the revival of full visual sensation and perception, because perception requires transmission of these signals to multiple higher visual centres of the brain, which was not possible using enucleated eyes.

The revival of human macular photoreceptors capable of generating light responses introduces the prospect of vision restoration using photoreceptor and/or macular transplantation from organ donors. This approach will face numerous challenges, such as inducing the integration of transplanted cells and patches into existing retinal circuitry, as well as overcoming the complications of retinal remodelling caused by retinal degeneration. These challenges are already under active research[46–50], although considerable research using animal models is required to assess the feasibility of this approach. Our results suggest that b-waves could be a sensitive biomarker to determine the viability of human retinal grafts. Finally, we have demonstrated that the use of ex vivo human donor retina is already a viable option for investigating the specific divergence of human neuronal function from that of animals and addressing the roadblocks to neuronal transplantation into the CNS and neuronal integration.

Online content

Any methods, additional references, Nature Research reporting summaries, source data, extended data, supplementary information, acknowledgements, peer review information; details of author contributions and competing interests; and statements of data and code availability are available at https://doi.org/10.1038/s41586-022-04709-x.

1. Borjigin, J. et al. Surge of neurophysiological coherence and connectivity in the dying brain. *Proc. Natl Acad. Sci. USA* **110**, 14432–14437 (2013).
2. Cole, S. L. & Corday, E. Four-minute limit for cardiac resuscitation. *J. Am. Med. Assoc.* **161**, 1454–1458 (1956).
3. Parnia, S., Waller, D. G., Yeates, R. & Fenwick, P. A qualitative and quantitative study of the incidence, features and aetiology of near death experiences in cardiac arrest survivors. *Resuscitation* **48**, 149–156 (2001).
4. Vrselja, Z. et al. Restoration of brain circulation and cellular functions hours post-mortem. *Nature* **568**, 336–343 (2019).
5. Iyer, A. et al. Pathophysiological trends during withdrawal of life support: implications for organ donation after circulatory death. *Transplantation* **100**, 2621–2629 (2016).
6. Donaldson, A. E. & Lamont, I. L. Biochemistry changes that occur after death: potential markers for determining post-mortem interval. *PLoS ONE* **8**, e82011 (2013).
7. Yu, D. Y. & Cringle, S. J. Oxygen distribution in the mouse retina. *Invest. Ophthalmol. Vis. Sci.* **47**, 1109–1112 (2006).
8. Zhu, S. et al. Impact of euthanasia, dissection and postmortem delay on metabolic profile in mouse retina and RPE/choroid. *Exp. Eye Res.* **174**, 113–120 (2018).
9. Wu, J. Y. & Prentice, H. Role of taurine in the central nervous system. *J. Biomed. Sci.* **17**, S1 (2010). **Suppl. 1**.
10. Ingram, N. T., Fain, G. L. & Sampath, A. P. Elevated energy requirement of cone photoreceptors. *Proc. Natl Acad. Sci. USA* **117**, 19599–19603 (2020).
11. Cowan, C. S. et al. Cell types of the human retina and its organoids at single-cell resolution. *Cell* **182**, 1623–1640.e1634 (2020).
12. Wang, J. S. & Kefalov, V. J. An alternative pathway mediates the mouse and human cone visual cycle. *Curr. Biol.* **19**, 1665–1669 (2009).
13. Schnapf, J. L., Kraft, T. W. & Baylor, D. A. Spectral sensitivity of human cone photoreceptors. *Nature* **325**, 439–441 (1987).
14. Kraft, T. W., Neitz, J. & Neitz, M. Spectra of human L cones. *Vision Res.* **38**, 3663–3670 (1998).
15. Huang, J. C., Voaden, M. J. & Marshall, J. Survival of structure and function in postmortem rat and human retinas: rhodopsin regeneration, cGMP and the ERG. *Curr. Eye Res.* **9**, 151–162 (1990).
16. Huang, J. C., Voaden, M. J., Marshall, J. & Kemp, C. M. Electrophysiologic characteristics of human and rat retinas in vitro. *Doc. Ophthalmol.* **76**, 27–35 (1990).
17. Huang, J. C., Arden, G. B., Voaden, M. J. & Marshall, J. Survival of cone responses in postmortem human retina. *Doc. Ophthalmol.* **83**, 91–96 (1993).
18. Kraft, T. W., Schneeweis, D. M. & Schnapf, J. L. Visual transduction in human rod photoreceptors. *J. Physiol.* **464**, 747–765 (1993).
19. Vinberg, F., Kolesnikov, A. V. & Kefalov, V. J. Ex vivo ERG analysis of photoreceptors using an in vivo ERG system. *Vision Res.* **101**, 108–117 (2014).
20. Nymark, S., Haldin, C., Tenhu, H. & Koskelainen, A. A new method for measuring free drug concentration: retinal tissue as a biosensor. *Invest. Ophthalmol. Vis. Sci.* **47**, 2583–2588 (2006).
21. Weinstein, G. W., Hobson, R. R. & Dowling, J. E. Light and dark adaptation in the isolated rat retina. *Nature* **215**, 134–138 (1967).
22. Winkler, B. S. The electroretinogram of the isolated rat retina. *Vision Res.* **12**, 1183–1198 (1972).
23. Granit, R. The components of the retinal action potential in mammals and their relation to the discharge in the optic nerve. *J. Physiol.* **77**, 207–239 (1933).
24. Masland, R. H. & Ames, A. 3rd Dissociation of field potential from neuronal activity in the isolated retina: failure of the b-wave with normal ganglion cell response. *J. Neurobiol.* **6**, 305–312 (1975).
25. Kim, H. M., Park, K. H. & Woo, S. J. Correlation of electroretinography components with visual function and prognosis of central retinal artery occlusion. *Sci. Rep.* **10**, 12146 (2020).
26. Reinhard, K. et al. Hypothermia promotes survival of ischemic retinal ganglion cells. *Invest. Ophthalmol. Vis. Sci.* **57**, 658–663 (2016).
27. Mure, L. S., Vinberg, F., Hanneken, A. & Panda, S. Functional diversity of human intrinsically photosensitive retinal ganglion cells. *Science* **366**, 1251–1255 (2019).
28. Raeburn, C. D., Cleveland, J. C. Jr, Zimmerman, M. A. & Harken, A. H. Organ preconditioning. *Arch. Surg.* **136**, 1263–1266 (2001).
29. Reinhard, K. & Munch, T. A. Visual properties of human retinal ganglion cells. *PLoS ONE* **16**, e0246952 (2021).
30. Soto, F. et al. Efficient coding by midget and parasol ganglion cells in the human retina. *Neuron* **107**, 656–666.e655 (2020).
31. Weinstein, G. W., Hobson, R. R. & Baker, F. H. Extracellular recordings from human retinal ganglion cells. *Science* **171**, 1021–1022 (1971).
32. Robson, J. G., Saszik, S. M., Ahmed, J. & Frishman, L. J. Rod and cone contributions to the a-wave of the electroretinogram of the macaque. *J. Physiol.* **547**, 509–530 (2003).
33. Kuchenbecker, J. A., Greenwald, S. H., Neitz, M. & Neitz, J. Cone-isolating ON–OFF electroretinogram for studying chromatic pathways in the retina. *J. Opt. Soc. Am. A* **31**, A208–A213 (2014).
34. Yan, W. et al. Cell atlas of the human fovea and peripheral retina. *Sci. Rep.* **10**, 9802 (2020).
35. Lu, Y. et al. Single-cell analysis of human retina identifies evolutionarily conserved and species-specific mechanisms controlling development. *Dev. Cell* **53**, 473–491.e479 (2020).
36. Kling, A. et al. Functional organization of midget and parasol ganglion cells in the human retina. Preprint at https://doi.org/10.1101/2020.08.07.240762 (2020).
37. Yi, W. et al. A single-cell transcriptome atlas of the aging human and macaque retina. *Nat. Sci. Rev.* **8**, nwaa179 (2020).
38. Fortenbach, C. R., Kessler, C., Peinado Allina, G. & Burns, M. E. Speeding rod recovery improves temporal resolution in the retina. *Vision Res.* **110**, 57–67 (2015).
39. Pepperberg, D. R. et al. Light-dependent delay in the falling phase of the retinal rod photoresponse. *Vis. Neurosci.* **8**, 9–18 (1992).
40. Gross, O. P. & Burns, M. E. Control of rhodopsin's active lifetime by arrestin-1 expression in mammalian rods. *J. Neurosci.* **30**, 3450–3457 (2010).

41. Krispel, C. M. et al. RGS expression rate-limits recovery of rod photoresponses. *Neuron* **51**, 409–416 (2006).
42. Owsley, C. et al. Psychophysical evidence for rod vulnerability in age-related macular degeneration. *Invest. Ophthalmol. Vis. Sci.* **41**, 267–273 (2000).
43. Curcio, C. A., Medeiros, N. E. & Millican, C. L. Photoreceptor loss in age-related macular degeneration. *Invest. Ophthalmol. Vis. Sci.* **37**, 1236–1249 (1996).
44. Sinha, R. et al. Cellular and circuit mechanisms shaping the perceptual properties of the primate fovea. *Cell* **168**, 413–426.e412 (2017).
45. van Hateren, J. H. & Lamb, T. D. The photocurrent response of human cones is fast and monophasic. *BMC Neurosci.* **7**, 34 (2006).
46. Pearson, R. A. et al. Restoration of vision after transplantation of photoreceptors. *Nature* **485**, 99–103 (2012).
47. Wang, T. et al. Activation of rod input in a model of retinal degeneration reverses retinal remodeling and induces formation of functional synapses and recovery of visual signaling in the adult retina. *J. Neurosci.* **39**, 6798–6810 (2019).
48. Telias, M. et al. Retinoic acid induces hyperactivity, and blocking its receptor unmasks light responses and augments vision in retinal degeneration. *Neuron* **102**, 574–586.e5 (2019).
49. Jones, B. W. et al. Retinal remodeling and metabolic alterations in human AMD. *Front. Cell. Neurosci.* **10**, 103 (2016).
50. Jones, B. W. et al. Retinal remodeling in human retinitis pigmentosa. *Exp. Eye Res.* **150**, 149–165 (2016).
51. Calvert, P. D. et al. Phototransduction in transgenic mice after targeted deletion of the rod transducin α-subunit. *Proc. Natl Acad. Sci. USA* **97**, 13913–13918 (2000).
52. Gurevich, L. & Slaughter, M. M. Comparison of the waveforms of the ON bipolar neuron and the b-wave of the electroretinogram. *Vision Res.* **33**, 2431–2435 (1993).
53. Bolnick, D. A., Walter, A. E. & Sillman, A. J. Barium suppresses slow PIII in perfused bullfrog retina. *Vision Res.* **19**, 1117–1119 (1979).
54. Sakami, S. et al. Probing mechanisms of photoreceptor degeneration in a new mouse model of the common form of autosomal dominant retinitis pigmentosa due to P23H opsin mutations. *J. Biol. Chem.* **286**, 10551–10567 (2011).
55. Marc, R. E., Murry, R. F. & Basinger, S. F. Pattern recognition of amino acid signatures in retinal neurons. *J. Neurosci.* **15**, 5106–5129 (1995).
56. Schindelin, J. et al. Fiji: an open-source platform for biological-image analysis. *Nat. Methods* **9**, 676–682 (2012).
57. Lamb, T. D. & Pugh, E. N. Jr A quantitative account of the activation steps involved in phototransduction in amphibian photoreceptors. *J. Physiol.* **449**, 719–758 (1992).
58. Smith, N. P. & Lamb, T. D. The a-wave of the human electroretinogram recorded with a minimally invasive technique. *Vision Res.* **37**, 2943–2952 (1997).

Methods

Animal handling and ethical statement

C57Bl6/J (wild-type) and *Gnat1*$^{-/-}$ mice[51] were bred in house or purchased at 8–10 weeks of age from Jackson Laboratory. All mice were housed within the University of Utah's animal facilities in standard housing with littermates. Mice were provided with food and water ad libitum, maintained on a 12 h:12 h (light:dark) cycle, at approximately 20% humidity and ~21 °C. All experiments were approved by the Institutional Animal Care and Use Committee of the University of Utah and conducted according to the ARVO Statement for the Use of Animals in Ophthalmic and Vision Research. Unless otherwise noted, all animals used were between 6–20 weeks old, and both males and females were used for experiments. Macaque (*M. fascicularis*) eyes were kindly provided by C. Faulkner and J. Perlmutter. Care of macaques was in accordance with the Guide for the Care and Use of Research Animals, and all experimental protocols were approved by the Washington University School of Medicine Animal Studies Committee.

Human tissue collection and ethical statements

Eyes were obtained from organ donors after a diagnosis of brain or cardiac death had been established by independent medical professionals according to the guidelines established by the Uniform Determination of Death Act (UDDA). All procedures related to human tissue procurement were carried out by representatives from Lifesharing, the Utah Lions Eye bank or the San Diego Eye bank, which are fully accredited for donor eligibility determination, recovery and distribution by the FDA, the Association of Organ Procurement Organizations (AOPO) and the Eye Banks of America Association (Utah Lions Eye Bank accreditation no. 0021114, and San Diego Eye Bank accreditation no. 0018106). All donor eyes were obtained with consent for research use according to the Uniform Anatomical Gift Act (UAGA) in the State of California or the Utah Lions Eye Bank. The research team was not involved with the identification or selection of organ donors, and all tissues were anonymized before transfer and could not be traced to specific donors. For this reason, the research was provided exempt status by the University of Utah (IRB no. 00106658) and ScrippsHealth IRB (IRB no. 16–6781). Exclusion criteria given to the eye banks included diagnoses with ocular disorders such as age-related macular degeneration and diabetes.

In vivo ERG recordings

We assessed light-evoked electrical activity of photoreceptors and ON bipolar cells using in vivo ERG in wild-type mice. Mice were dark adapted overnight and anaesthetized for 20 min with 2% isoflurane in room air using a SomnoSuite Low Flow Anesthesia System (Kent Scientific). Pupils were dilated with 2% atropine sulfate eye drops (Akorn Pharmaceuticals) and corneas were lubricated with a mixture of phosphate-buffered saline (PBS) with Goniovisc (2.5% hypromellose solution, Contacare). Euthanasia was by cervical dislocation, and recording started within 30 s of death. ERG waveforms were recorded using corneal contact lens electrodes, a subdermal needle electrode inserted between the eyes was the reference electrode, a subdermal needle at the base of the tail as the ground electrode. For intravitreal injections, mice were anaesthetized with ketamine/xylazine, and pupils dilated with 1% atropine eye drops (Akorn). A 30G subdermic needle was used to create a pilot hole, through which a blunt 33 Gauge Hamilton needle (7803-05, Hamilton) was advanced. To isolate photoreceptor component from the inner retinal components (mainly generated by ON bipolar cells[52]), a 1 µl volume of DL-AP4 solution (1.6 mM in PBS) was injected from a Hamilton syringe (5 µl Microliter Syringe Model 65 RN, Hamilton) into the vitreous. Responses to flash intensities of 10 cd s m^{-2} every 5 s (525 nm wavelength) were collected using a ColorDome (Diagnosys) and Espion V6 software.

Ex vivo electroretinogram recordings

Wild-type or *Gnat1*$^{-/-}$ mice were dark-adapted overnight (8–12 h), before euthanasia by CO_2 inhalation and cervical dislocation. All procedures after dark adaptation were performed under dim red light. Eyes were enucleated into freshly prepared Ames media (A1420, Sigma-Aldrich) bubbled with 5% CO_2/95% O_2 unless otherwise stated. Eyes were hemisected, lens and cornea removed, and retina isolated from the eyecup.

Ex vivo ERG recordings were performed as described[19]. Isolated retinas were mounted photoreceptor side up onto the specimen holder (Extended Data Fig. 3) and perfused with Ames supplemented with $BaCl_2$ (ref.[53]) (100 µM; 342920, Sigma-Aldrich) and DL-AP4[52] (40 µM, Tocris Bioscience) to isolate the photoreceptor component of the ERG signal (a-wave) from inner retina contributions originating mainly from ON bipolar cell activity (b-wave). ON bipolar cell component was derived by subtracting responses recorded in presence of DL-AP4 from those recorded in the absence of DL-AP4. The perfusion rate was ~2 ml min^{-1}, perfused media was temperature controlled at 37 °C and bubbled with a 95% O_2 and 5% CO_2 mix.

ERG signal was first amplified (100×) and low-pass filtered at 300 Hz by a differential amplifier (DP-311, Warner Instruments), and data were further amplified (10×) and acquired at 10 kHz using an integrated Sutter IPA amplifier/digitizer (IPA, Sutter Instrument). Light stimuli were provided either from a high-power LED light source (Solis-3C, Thorlabs), with filter for green light and LED driver (DC2200, Thorlabs), or a high-power LED light source (LED4D067, 530 nm, Thorlabs). Light stimulus durations ranged from 2–20 ms. The SutterPatch software (SutterPatch v1.1.2–2.0.2, Sutter Instrument) drove both stimulus generation and data acquisition via the IPA amplifier's analogue output and input, respectively. For experiments comparing human rod and cone physiology, a yellow filter (560 nm center wavelength, 10 nm full width at half maximum; FB560-10, Thorlabs) was fitted to a high-powered LED light source.

To isolate cone responses in human retina, double flash stimuli were selected whereby the first flash would saturate rods (~25,000 photons µm^{-2}) and the second flash to stimulate cones was presented 500 ms after the saturating flash (Extended Data Fig. 7). In macaque experiments, the rod-saturating flash was ~15,000 photons (500 nm) µm^{-2}, and the second flash to stimulate cones was presented 300 ms after the saturating flash, or in some experiments ~5,000 photons (500 nm) µm^{-2} background light was used to suppress rod responses. Light stimuli were calibrated before experiments using a calibrated photodiode (FDS100-CAL, Thorlabs) and flash intensities converted to photons µm^{-2}.

Effect of death-to-enucleation delay on photoreceptor and ON bipolar cell function

For experiments simulating the effect of death-to-enucleation delay on the ERG, wild-type or *Gnat1*$^{-/-}$ mice were euthanized as above. Enucleation was delayed by 15 min to 3 h, or control eyes were enucleated immediately after euthanasia. Ex vivo ERG was then carried out using either Ames + $BaCl_2$ to measure bipolar cell responses with photoreceptor responses, or Ames + $BaCl_2$ + DL-AP4 to measure photoreceptor responses in isolation. Subtraction of the pharmacologically isolated photoreceptor responses from the responses of the photoreceptors combined with bipolar cells provides the amplitude of the bipolar cell response.

Effect of low pH and low oxygen on bipolar cell function

For experiments simulating the effect of postmortem hypoxia, we compared light responses between standard conditions where the perfusion solution was continuously bubbled with standard 95% O_2/5% CO_2 gas mixture to one where most of the oxygen was replaced by nitrogen (N_2). When we saturated our Ames medium with 95% O_2/5% CO_2, 80% PO_2 was measured with an oxygen microelectrode at the retina (ET1120 Micro

Oxygen Electrode, eDAQ), whereas when perfusing with 95% N_2/5% CO_2, the PO_2 dropped to 2.5% at the retina. For experiments comparing the effect of low pH on ERG b-waves, we titrated the concentration of sodium bicarbonate in the Ames perfusion solution used until a pH of ~6.8 was achieved under the conditions maintained during incubation or perfusion. In both conditions, retinas were perfused with the modified (low pH or low oxygen) or control Ames solutions that contained 100 μM $BaCl_2$ to remove ERG component originating from Müller cells[53], and responses to a stimulus 90 photons (505 nm) μm^{-2} were measured over the course of 60 min. ERG b-wave amplitudes from these responses were measured from the negative a-wave peak to the positive b-wave peak (peak-to-peak height).

To understand if changes in the ON bipolar cell function is reversible, we incubated the entire eye in Ames of either low pH or low O_2, obtained as described above, between 15 min to 3 h, with control eyes incubated for the same period in pH 7.4 Ames bubbled with 95% O_2/5% CO_2 gas mixture. Since eyes for low oxygen experiments were bathed in Ames medium saturated continuously with 95% N_2/5% CO_2 in a closed container, we expect that they were exposed to 0% O_2 for the duration of the incubation. Following this initial incubation in low pH/low O_2, or control conditions, the retinas were dissected, mounted in the ex vivo ERG specimen holder, and perfused for 20 min (low O_2 experiments) or one hour (low pH experiments) with warmed Ames bubbled with 95% O_2/5% CO_2. Following this perfusion period in normal Ames containing 100 μM $BaCl_2$, we measured responses to light stimuli of 30 photons (505 nm) μm^{-2} from the retina to measure the recovery of responses. ERG b-wave amplitudes were measured from these responses from negative a-wave peak to the positive b-wave peak (peak-to-peak height).

Human organ donor and macaque ex vivo ERG

Enucleated eyes from three individual macaques (*Macaca fascicularis*) that were used in other research projects were obtained after their scheduled euthanasia with a lethal overdose of pentobarbital (>150 mg kg^{-1} intravenously). Ex vivo ERG experiments were conducted in a laboratory that was ~10 min walking distance from the location of euthanasia. Macaques were not dark-adapted prior to euthanasia, and bright surgical lights were used during eye enucleation. Thus, to promote pigment regeneration and dark adaptation of photoreceptors, we incubated the whole eyeballs in oxygenated Ames media for 20–30 min in a light-proof container. This may not have been enough to ensure a complete dark adaptation of rod photoreceptors but was a compromise to minimize total postmortem time and to support cone dominance in the ex vivo ERG signal. After incubation, cornea, lens, and most of the vitreous was removed in the dark before a 6 mm patch of the retina was taken centered at the fovea. These macular patches were placed on a custom-built ex vivo ERG specimen holder with a 2 mm effective recording area. Responses were recorded to a homogenous 5 mm spot of light completely covering the recording area.

Five pairs of human organ donor eyes were recovered within 20 min after circulatory arrest from donation after brain death donors who were maintained on life support prior to organ donation (n = 5 donors, see Supplementary Table 3). An additional three pairs of human organ donor eyes were recovered within 45 min and 2 h from donation after cardiac death (DCD) donors who were maintained on life support prior to cardiac death (n = 3 donors, see donors 1–3 in Supplementary Table 3). Whole globes were stored in a light-tight container in bicarbonate buffered Ames for transportation and bubbled with 100% O_2 during transportation to the lab (see Fig. 3a), after which they were incubated in Ames bubbled with 95% O_2/ 5% CO_2. All subsequent procedures were carried out under dim red light. The lens and cornea were removed from the globe. Several punches were taken from the peripheral retina using a 5 mm biopsy punch, and a single punch was taken centred on the fovea. These large punches were then divided into pieces ~2 mm in diameter to completely cover the 0.5 mm recording aperture of the ex vivo ERG specimen holder (see Extended Data Fig. 3). The neural retina was separated from retinal pigment epithelium (RPE) and choroid. Each retinal punch was perfused in the specimen holder with Ames containing 100 μM $BaCl_2$ bubbled with 95% O_2 and 5% CO_2 and warmed to 37 °C during experiments.

Human research donor eye ex vivo ERG experiments

Anonymized research donor eyes were obtained from the Utah Lions Eye Bank (n = 17 pairs; Supplementary Table 4) between 2–5 h postmortem. Whole globes were stored in bicarbonate buffered Ames in the dark after enucleation and during transport and allowed to dark-adapt a further 30–60 min (depending on transport time). The lens and cornea were removed from the eye, and a 6 mm biopsy punch was used to take tissue punches from either the macula or peripheral retina. Neural retina was then separated from the underlying RPE and choroid. Each retinal punch was mounted in a custom-built specimen holder, with recording area of 2 mm in diameter, and perfused with Ames containing 100 μM $BaCl_2$ bubbled with 95% O_2 and 5% CO_2 and warmed to 37 °C during experiments.

Immunohistochemistry of the postmortem retina

Wild-type or $P23H^{+/-}$ mice[54] (positive control) were euthanized according to IACUC guidelines. Control eyes were enucleated immediately or delayed for 45 or 180 min before enucleation in the dark. All eyes were then fixed for 10 min in 4% paraformaldehyde (PFA) with 30% glucose phosphate-buffered saline (PBS), the cornea was punctured, and a second 10 min 4% PFA fixation was carried out. Eyes were washed in PBS and the cornea and lens removed. Eyecups were cryoprotected for 30 min at room temperature in 15% sucrose PBS before incubation in 30% sucrose PBS overnight at 4 °C. Eyecups were then embedded in OCT medium (Tissue-Tek, Sakura Finetek) 12-μm sections were mounted on slides. To minimize differences in staining that could be attributed to sample preparation, eyecups from two separate treatment groups were mounted on each slide. Slides were blocked with 10% normal goat serum (NGS) in 0.1% PBS-Triton-X for one hour at room temperature before incubating with Anti-activated Caspase-3 antibody (catalogue no. 559565, 1:500 dilution, BD Pharmingen; Supplementary Table 5) in blocking buffer overnight at 4 °C. Slides were washed in PBS before incubating in secondary antibody (Goat anti-Rabbit Alexa 594, 1:1,000, Invitrogen) at room temperature for one hour. Slides were then mounted with a coverslip and Fluoromount-G mounting medium with DAPI (Invitrogen, Catalog 00-4959-52, Invitrogen). Images were acquired on an Olympus confocal (FV1000, Olympus Scientific Solutions) running Olympus Fluoview v4.2.3.6, with a 40× oil immersion objective (Olympus UAPO 40× oil immersion, NA 1.35, Olympus Scientific Solutions) at 640 × 640 pixel resolution (pixel size = 0.497 μm^2). Imaging settings were optimized to the fluorescence signal on a positive control slide ($P23H^{+/-}$ retina, 21 days old), and then maintained for the rest of the slides. A single image was taken from several sections from each eye in each condition, and the number of activated caspase-3-labelled cells in each retinal section averaged for each mouse, which was then used to calculate an average for each condition.

Computational molecular phenotyping

Wild-type mice of both sexes at 2 months old were euthanized by deep isoflurane anaesthetization followed by decapitation, according to IACUC guidelines, and either enucleated immediately (control) or after a 45 min postmortem delay. Methods have been described[55]. In brief, eyes were enucleated and fixed in buffered 2.5% glutaraldehyde/1% formaldehyde overnight, before resin embedding and serial sectioning. The sections were probed with IgGs for small molecules (see Supplementary Table 6 for list), including glutamate (E), glutamine (Q), and taurine (TT). Subsequent visualization was with secondary antibodies conjugated to 1.4 nm gold (catalogue no. 2300, Nanoprobes), followed by silver intensification.

Images were captured as 8-bit high resolution (243 nm per pixel) images and registered with ir-tweak v1.4 (https://www.sci.utah.edu/download/ncrtoolset.html) into image databases. Adobe Photoshop CC (Adobe) was used for final image generation. For display only, raw data channels are linearly contrast-stretched. Molecular signals were visualized as selected RGB maps encoding taurine, L-glutamine and L-glutamate to red, green, and blue colour channels. Masks were created to isolate bipolar cell bodies, Muller cells in the outer nuclear layer, photoreceptor cell bodies, and photoreceptor outer segments, to prevent contamination of signal from other cell populations. Monochrome images are density mapped. Histograms were taken from an area of the retina spanning 200 µm wide for each retina sampled. CMP images were prepared in Adobe Photoshop CC (Adobe), and histograms of pixel intensities were measured in FIJI[56].

Data analysis

Data analysis, including statistical analysis and figure prepared in Origin 2018 (OriginLab) and edited in Adobe Illustrator CC (Adobe). Normalized responses are calculated for each retina by dividing the response amplitude data (R) by the maximal amplitude measured at the peak/plateau of the response (R_{max}) to the brightest flash (R/R_{max}).

Dominant time constants (τ_D) for macular and peripheral photoreceptors were calculated by measuring the time taken for saturated photoreceptor responses to return to a threshold level (50% of saturated response amplitude for cones, 70% of saturated response amplitude for rods). These values were then plotted against the natural logarithm of the flash intensities used, and a linear fit (equation (4)) was used to determine the slope, τ_D, which defines the lifetime of the longest living phototransduction protein in the photoreceptor. Cone photoreceptors are harder to saturate, and specifically from the peripheral retina we did not always have enough saturated responses to generate a reliable linear fit for the ln(I) vs T_{sat} plot. Thus, we sometimes included one or two light responses that were not quite saturated and set the recovery threshold at 50% of the maximal photoresponse (R_{max}) for all the subsequent analysis. The selection of a different thresholds does not change the τ_D calculated from the slope of the linear fit to ln(I) vs T_{sat} data, which we confirmed by also performing analysis using 70% threshold in macular cones (data not shown).

Statistics and reproducibility

All representative plots shown were reproduced more than three times from the same retina (technical replicates) and across animals (biological replicates). Normal inter-animal differences in response amplitudes were recorded, but do not alter conclusions made in this Article and are all presented within graphs. Statistical differences between different experimental groups were analysed by a one-way ANOVA with Holm–Bonferroni means comparisons test where appropriate. Comparisons of linear fits were carried out with the F-test, with $P < 0.05$ considered a significantly different fit. Data are presented as mean ± s.e.m., unless otherwise noted in figure legends. A value of $P < 0.05$ is considered significant. N numbers as animals/donors, retinas or retinal pieces are noted in the figure legends. Degrees of freedom and F values, adjusted R^2 and Pearson's R are reported in the figure legends. For experiments in mice no statistical sample size calculation was performed. Sample sizes were based on prior experience of suitable n numbers with a minimum of n of 3 animals for each condition. Retinal responses to different intensities of light were replicated by taking multiple responses from each retina to each light intensity measured (minimum 3 repeats taken for each intensity used). Responses from each retina replicated successfully and the average of these replicated responses was used for analyses. Each experiment was repeated in multiple animals (n numbers reported in figures) across multiple experimental days. Replication of results was successful for all mouse experiments. For analyses of pH and hypoxia effects, an eye from each animal, of random sex, was randomly allocated to a condition group (controls/low pH/low O^2 / enucleation delay between 15 min to 3 h). It was not possible to blind investigators to postmortem delay time, pH or hypoxia condition or control groups during mouse ex and in vivo ERG data collection. However, investigators were blinded during analyses until summary statistics/condition group comparisons were carried out. For IHC and CMP acquisition and analyses investigators were blinded until summary statistics/condition group comparisons. We did not have biological replicates for human retinal experiments since almost all samples had a unique enucleation delay. For analysis of dominant times constant, kinetics and sensitivity parameters from organ donations after brain death we had a minimum of 2 biological replicates and 5 technical replicates for both macula and periphery. It was not possible to completely blind researchers to research donor enucleation delays during data collection since this information was provided by eye banks prior to acceptance of tissues.

Equations

To determine the amplification constant for the dim responses of both rod and cones in the postmortem retinas, we fitted to the initial rising phase of dim responses from both wild-type and *Gnat1*$^{-/-}$ mouse retinas to a model function to describe the kinetics of phototransduction activation[57]. The model may not accurately describe the kinetics of cone responses[58], but was used here to quantify and compare activation kinetics between immediate and postmortem delayed cones. Here, t_d is a small delay corresponding to the small delay in recording of responses, as well as delays in phototransduction, and A is the amplification constant in s^{-2}. Both t_d and A were allowed to vary to provide the best fit to the early rising phase of a dim flash response. Only intensity (Φ) was fixed to the intensity of light used (for wild-type retinas: 27 photons per µm^2; for *Gnat1*$^{-/-}$ retinas: 1,010 photons per µm^2).

This model is described by Lamb–Pugh activation kinetics (equation (1)),

$$\frac{R(t)}{R_{max}} = 1 - \exp\left(-\frac{1}{2}\Phi A(t - t_d)^2\right) \quad (1)$$

The results were fitted to response amplitude data to determine flash strength (I in photons µm^{-2}) producing 50% of R_{max} ($I_{1/2}$) using a Naka–Rushton function (equation (2)),

$$\frac{R}{R_{max}} = \frac{I}{I + I_{1/2}} \quad (2)$$

or a Hill function (equation (3)):

$$R = R_{max}\frac{I^n}{I^n + I_{1/2}^n} \quad (3)$$

A linear function to determine the average lifetime of the longest-living activated phototransduction protein (τ_D) [39]:

$$T_{sat} = \tau_D \times \ln(I) + b \quad (4)$$

This linear function was fitted to the saturated response recovery times (T_{sat}) to the threshold level (that is, 70% of the maximal response for rods, 50% for cones), and plotted against the natural logarithm of light flash intensity used, as described[39].

Reporting summary

Further information on research design is available in the Nature Research Reporting Summary linked to this paper.

Data availability

The data that support the findings of this study are available from G-Node at https://doi.org/10.12751/g-node.sayvud. Source data are provided with this paper.

Acknowledgements This work was supported by National Institutes of Health (P30 EY014800), and an Unrestricted Grant from Research to Prevent Blindness to the Department of Ophthalmology and Visual Sciences, University of Utah. A.H. is supported by NIH/NCATS grant UL1 TR002550, NIH EY031706, the Daro Foundation, the A. C. Israel Foundation, the Warren Family Foundation, the Renaissance Charitable Foundation, The Rancho Santa Fe Foundation, the Money Arenz Foundation, the Considine Foundation, the Fonseca Foundation, the Pfeiffer Foundation, the Mericos Eye Institute, the Thomas and Audrey Pine Foundation and additional philanthropic funding. F.V. is supported by NIH grant EY031706, Research to Prevent Blindness/Dr. H. James and Carole Free Career Development Award, Diabetes Research Connection, and International Retinal Research Foundation. S.B. is supported by ARVO Foundation for Eye Research EyeFind research grant. B.W.J. is supported by the National Institutes of Health (R01 EY015128, R01 EY028927) and the National Science Foundation (2014862). S.P. is supported by the National Institutes of Health (R01s: CA236352, DK115214, DK118278), Department of Defense (W81XWH1810645), and Wu-Tsai Human Performance Alliance and the Joe and Clara Tsai Foundation. L.S.M. is supported by Velux Stiftung. Figure schematics were made with resources from Biorender.com. We thank J. Dessert for producing the surgical donation and transportation illustrations in Fig. 3a; J. R. Allen for the fusion 360 model of the ex vivo ERG specimen holder in Extended Data Fig. 3; T. Neikirk, a member of the Hanneken laboratory, for providing technical support and assistance; H. Calligaro, a member of the Panda laboratory, for useful discussions of some of the most recent human retina experiments; C. Faulkner and J. Perlmutter for providing non-human primate eyes; the Utah Lions Eye Bank, Lifesharing and the San Diego Eye bank for providing human donor eyes. Finally, we are deeply grateful to those who donated their eyes, and their legal representatives who accommodated the surgical team's effort to procure the eyes.

Author contributions A.H. and F.V. conceived, organized and supervised the project. S.B. carried out and analysed mouse in vivo ERG and low-oxygen ex vivo ERG experiments. F.A. collected and analysed death-to-enucleation delay and low pH mouse ex vivo ERG data and carried out mouse immunohistochemistry staining and imaging. B.W.J. carried out and analysed CMP staining. F.A. and F.V. collected and analysed human research donor data. A.H. recovered the organ donor eyes. F.A., F.V. and L.S.M. acquired and analysed human organ donor data. F.V. acquired and analysed macaque data. F.A. and F.V. prepared the figures. F.A., A.H., S.P. and F.V. wrote the manuscript. All authors discussed and commented on the data.

Competing interests The authors declare no competing interests.

Additional information

Supplementary information The online version contains supplementary material available at https://doi.org/10.1038/s41586-022-04709-x.

Correspondence and requests for materials should be addressed to Anne Hanneken or Frans Vinberg.

Peer review information *Nature* thanks Michael Gorin, Andrew Huberman and the other, anonymous, reviewers for their contribution to the peer review of this work.

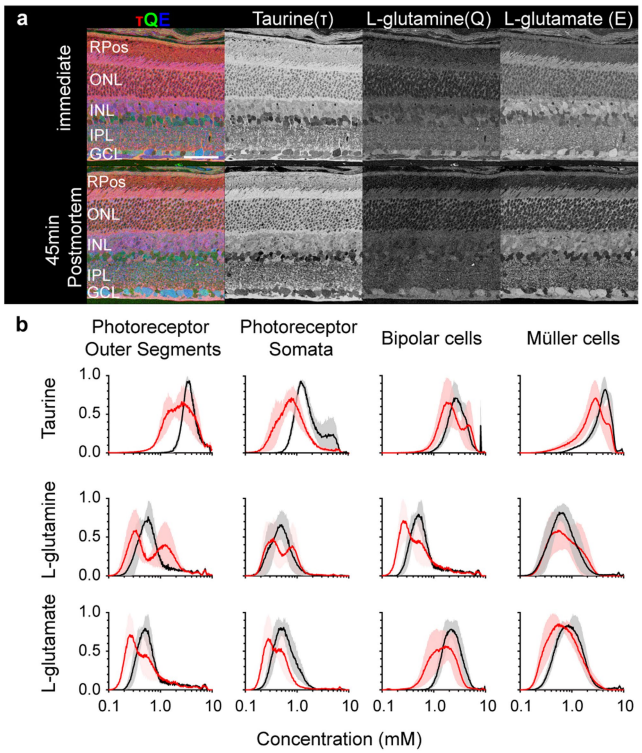

Extended Data Fig. 1 | Changes after 45 min death-to-enucleation delay to metabolites related to cell health and synaptic signaling. Example RGB maps of CMP staining of metabolites in the immediately fixed vs. 45-minute postmortem wild-type retina (**a**). τQE (Taurine, Glutamine, Glutamate) → RGB for both immediate and 45 min PM retinas. The density maps for each metabolite are also shown (greyscale). Scale bar represents 50 µm. Histograms of the mean levels of Taurine, Glutamine and Glutamate measured in retinas either after immediate enucleation (black) or 45 min enucleation delay (red, **b**), according to masked cell populations (n = 3 retinas from 3 animals). Data are presented as averages (lines) ± SEM (shaded areas).

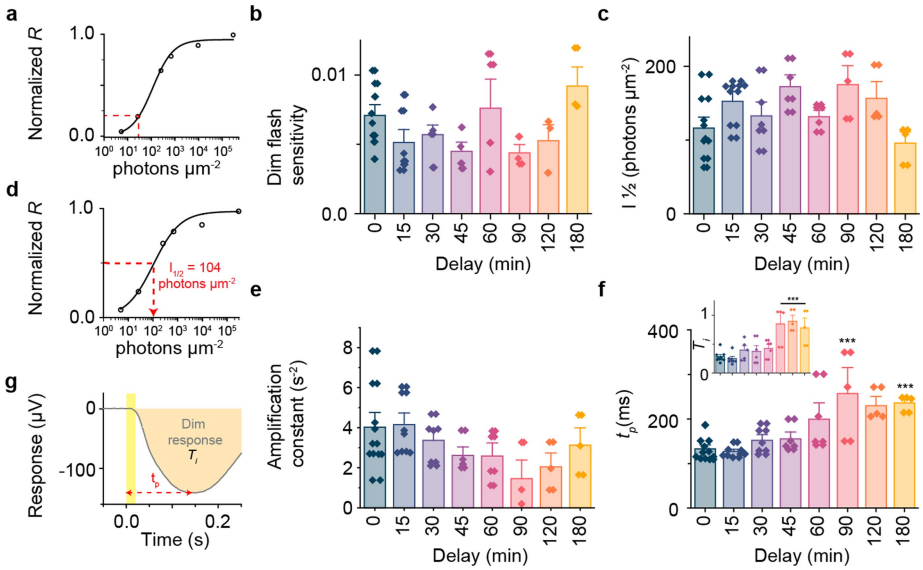

Extended Data Fig. 2 | Phototransduction sensitivity and kinetics in relation to enucleation delay. Example plot showing how dim flash response sensitivity is calculated **(a)**. Responses normalized to maximal response of retina plotted against the intensity of light stimulus, curve fits Naka-Rushton function (Eq. 2) to amplitude data, dim flash sensitivity is defined as response amplitude divided by R_{max} at constant intensity producing ~20% of the maximal response amplitude. Dim flash sensitivities of retinas from wild-type mouse retinas with different enucleation delays **(b)**, and $I_{1/2}$ values from retinas of wild-type mice with different enucleation delays **(c)**. Example response plot showing how $I_{1/2}$ was obtained **(d)**, responses of retina to each intensity presented is plotted and a Naka-Rushton fit applied to the plot. $I_{1/2}$ is the intensity required to produce half the maximal response size. Amplification constant plotted against enucleation delay for each retina **(e)**. Time-to-peak (t_p) and integral (T_i, inset) of dim responses for each retina plotted against the enucleation delay (**f**, *** indicates $p < 0.001$ compared to 0min). Exact p values: t_p: 0 vs 90 min p = 0.0002, 0 vs 120 min p = 0.002, 0 vs 180 min p = 0.001, T_i: 0 vs 90 min p = 0.002, 0 vs 120 min p = 0.0007, 0 vs 180 min p = 0.01). Example dim flash response showing how time-to-peak (t_p) and integration time (T_i) was calculated **(g)**. Time-to-peak is the time from light stimulus onset to the peak of the dim flash response. Integral (T_i) is the area under the dim flash response curve (orange shaded area), divided by the response amplitude. Light stimulus is indicated with a shaded yellow area. For all plots, bar height indicates mean, error bars represent ± SEM. All comparisons are one-way ANOVA with Holm-Bonferroni means comparisons. (DF: 35 for all comparisons, F values: Ti = 8.4, t_p = 5.8, Dim flash sensitivity = 2.0, Amplification constant = 1.6, $I_{1/2}$: 2.2).

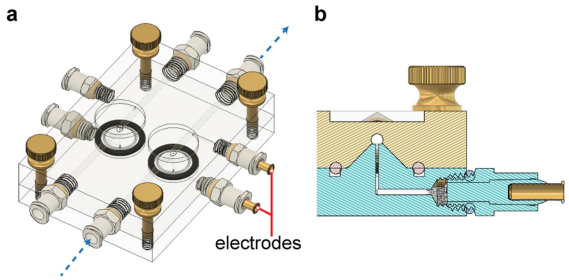

Extended Data Fig. 3 | Drawings of *ex vivo* ERG specimen holder for CNC machining from polycarbonate. (exported from Fusion 360, Autodesk, used to design the specimen holder for CNC machining). Retina samples are placed on the dome (shaded in blue in **b**). The dome has electrode channel with Ø0.5–2 mm diameter that determines the recording area. O-ring (a, black shading; b, pink shading) minimizes shunt currents to improve signal-to-noise ratio (SNR).

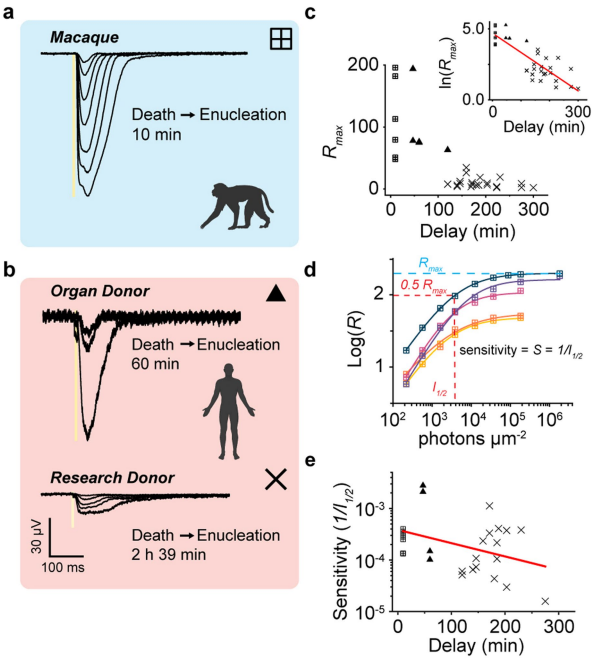

Extended Data Fig. 4 | Comparison of freshly enucleated Macaque retina, and human organ and research donor maculas with longer enucleation delays. Light responses of macular cones from freshly enucleated macaque (**a**, hatched squares, n = 5 maculae, from 3 animals) human DCD donor (**b**, filled triangles, **top trace**, n = 5 maculae from 3 donors) and research donor eyes (**b**, crosses **lower trace**, n = 23 maculae from 17 donors). (**c**) The maximal response obtained from maculae from each tissue type plotted against enucleation delay. Inset shows Ln of R_{max} from each macula, and linear fit in red with decay (τ = 74 min). (**d**) Example of how sensitivity, S ($1/I_{1/2}$), is calculated. Macular responses to different light intensities were plotted and a Hill curve fitted (see Eq. 3 in Methods) to determine the intensity required to produce a half-maximal response size. (**e**) Sensitivities of each macula plotted against enucleation delay, linear fit in red (no significant correlation between delay and S, ANOVA, DF =24, F value = 3.9, p = 0.06).

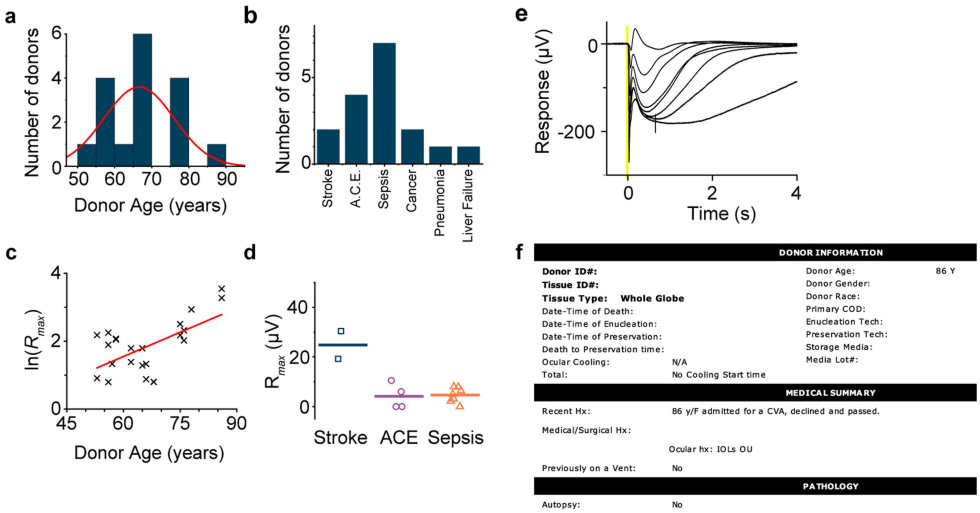

Extended Data Fig. 5 | Contributing factors to the quality of light-evoked responses from human postmortem research donor retinas. (**a**) Histogram of research donor ages, with numbers of donors represented within the bars. (**b**) Histogram of the primary cause of death of donors as noted on tissue donor forms. (**c**) The maximal response obtained from each donor eye plotted against donor age, with linear fit showing a positive correlation (n = 23 maculae, Pearson's r = 0.61, adjusted $R^2 = 0.37$) (**d**) Average maximal amplitude obtained from each research donor according to the primary cause of death (Stroke: squares, n = 2 donors, ACE: circles, n = 4 donors, Sepsis: triangles, n = 7 donors), data are averages of responses obtained from each individual donor, with mean presented as a solid line. Maculae that did not produce any detectable responses were included as a response size of 0 µV. Donor information (**e**) for a single donor (donor #8) in which *ex vivo* ERG ON-bipolar cell responses were recorded to flash intensities of 29–32,500 photons μm^{-2} (**f**). Yellow bar indicates the onset of flash stimuli.

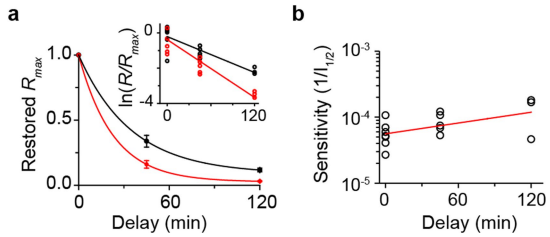

Extended Data Fig. 6 | Decay of cone photoreceptor and bipolar cell function in relation to the enucleation delay in Gnat1$^{-/-}$ mice. (**a**) The R_{max} of mouse cone photoreceptors (black circle) and bipolar cells (red circle) plotted as a function of enucleation delay, normalized to maximal response obtained with 0 min enucleation delay. Smooth traces plot exponential decay function fitted to mean data. Inset plots natural log amplitude data for individual retinas (τ = 53 min for photoreceptors, τ = 35 min for bipolar cells), and linear fit (Photoreceptor fit: Pearson's r = −0.851 with adj. R^2 = 0.704, Bipolar cell fit: Pearson's r = 0.905 with adj R^2 = 0.819). Sensitivity of retinas at different enucleation delays (**b**, $1/I_{1/2}$), Pearson's r = 0.52 with adj. R^2 = 0.27. For all plots, n (retinas, animals) is 0min = 7, 45 min = 5, 120 min = 3, responses from individual retinas are plotted as hollow circles.

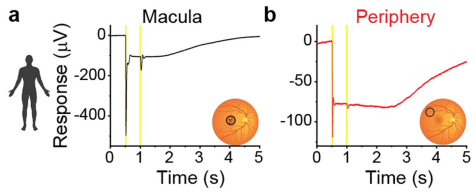

Extended Data Fig. 7 | Double-flash responses allow the isolation of cone responses from rod in both human macula (a) and periphery (b). Representative responses from human donor macular (**a**, black) and peripheral (**b**, red) punches to double-flash light stimuli to isolate cone responses. Light flashes are indicated with yellow shading, rod saturating flash intensity was ~25,000, cone stimulating intensities used were 2800–147,000 photons (560 nm) μm^{-2}.

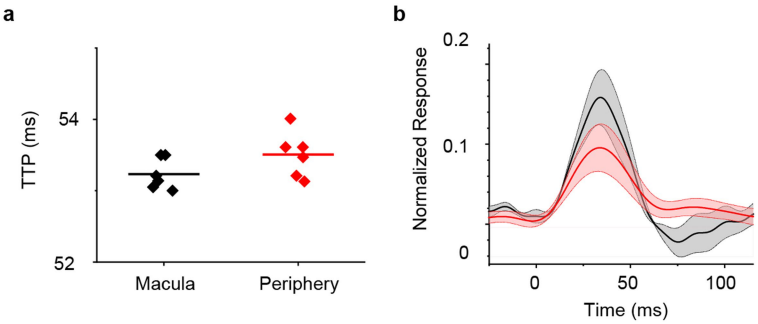

Extended Data Fig. 8 | Comparison of Human Macular and Peripheral Cone sensitivity and kinetics. Dim flash response time-to-peak (at intensity producing response size 15–20% of maximal retina response in ms) recorded from human macular and peripheral cone responses (**c**), individual responses are shown as diamonds, with line indicating mean. The average dim flash photoreceptor response normalized to maximal response recorded from each retina, plotted against time (d). Graph line shows average response with shaded area showing ± SEM.

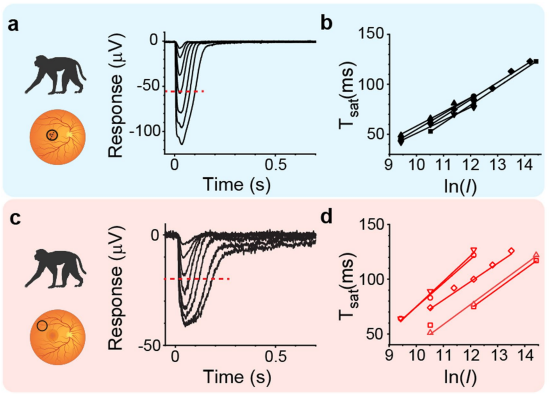

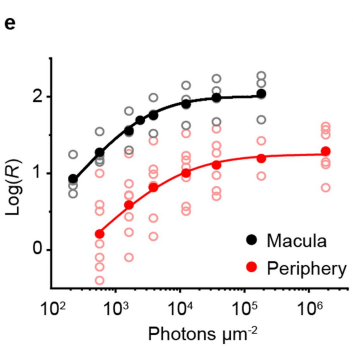

f

	Macula τd (ms)	Periphery τd (ms)
	15	22
	14	23
	13	17
	17	18
	18	18
Mean	15.4 ±0.93	19.6 ±1.21

Extended Data Fig. 9 | Determination of dominant time constant (τ_D) for macaque cones. Representative responses to flashes of light ranging from 220 to 183,000 photons (500 nm) μm^{-2} from a macular (**a**) and peripheral (**c**) sample recorded using *ex vivo* ERG. A rod-saturating pre-flash (15,000 photons μm^{-2} at 500 nm) was used to isolate cones in peripheral samples. Saturation times (T_{sat}) measured at 50% recovery (example red dashed line in **a, c**) plotted as a function of logarithmic light flash intensity (in photons μm^{-2}) for induvial macular (**b**) and peripheral samples (**d**). **e**. Log response amplitudes plotted against light intensities in macaque maculae (black) and peripheral retina punches (red) with Hill function fits (Eq. 3 in Methods) . n = 5 macular and n = 7 peripheral punches from 3 animals. (**f**) Table of statistics for slopes in (**b, d**), i.e. τ_D, mean ± SEM.

nature portfolio

Corresponding author(s): Frans Vinberg

Last updated by author(s): Jan 10, 2022

Reporting Summary

Nature Portfolio wishes to improve the reproducibility of the work that we publish. This form provides structure for consistency and transparency in reporting. For further information on Nature Portfolio policies, see our Editorial Policies and the Editorial Policy Checklist.

Statistics

For all statistical analyses, confirm that the following items are present in the figure legend, table legend, main text, or Methods section.

n/a	Confirmed	
☐	☒	The exact sample size (*n*) for each experimental group/condition, given as a discrete number and unit of measurement
☒	☐	A statement on whether measurements were taken from distinct samples or whether the same sample was measured repeatedly
☐	☒	The statistical test(s) used AND whether they are one- or two-sided *Only common tests should be described solely by name; describe more complex techniques in the Methods section.*
☐	☒	A description of all covariates tested
☐	☒	A description of any assumptions or corrections, such as tests of normality and adjustment for multiple comparisons
☐	☒	A full description of the statistical parameters including central tendency (e.g. means) or other basic estimates (e.g. regression coefficient) AND variation (e.g. standard deviation) or associated estimates of uncertainty (e.g. confidence intervals)
☐	☒	For null hypothesis testing, the test statistic (e.g. *F*, *t*, *r*) with confidence intervals, effect sizes, degrees of freedom and *P* value noted *Give P values as exact values whenever suitable.*
☒	☐	For Bayesian analysis, information on the choice of priors and Markov chain Monte Carlo settings
☒	☐	For hierarchical and complex designs, identification of the appropriate level for tests and full reporting of outcomes
☐	☒	Estimates of effect sizes (e.g. Cohen's *d*, Pearson's *r*), indicating how they were calculated

Our web collection on statistics for biologists contains articles on many of the points above.

Software and code

Policy information about availability of computer code

Data collection	Data were collected using Sutterpatch v1.1.2 - 2.0.2 (Sutter Instrument, CA, USA), Olympus Fluoview v4.2.3.6 (Olympus Scientific Solutions), in vivo ERG data collected with Espion v6 (Diagnosys LLC, Lowell, MA, USA)
Data analysis	Analyses were carried out using Origin 2018 (OriginLab, MA, USA), image analyses were done in FIJI (ImageJ v1.53c), CMP registration was carried out using ir-tweak v1.4 (https://www.sci.utah.edu/download/ncrtoolset.html)

For manuscripts utilizing custom algorithms or software that are central to the research but not yet described in published literature, software must be made available to editors and reviewers. We strongly encourage code deposition in a community repository (e.g. GitHub). See the Nature Portfolio guidelines for submitting code & software for further information.

Data

Policy information about availability of data

All manuscripts must include a data availability statement. This statement should provide the following information, where applicable:

- Accession codes, unique identifiers, or web links for publicly available datasets
- A description of any restrictions on data availability
- For clinical datasets or third party data, please ensure that the statement adheres to our policy

The data that support the findings of this study are available at https://doi.org/10.12751/g-node.sayvud

Field-specific reporting

Please select the one below that is the best fit for your research. If you are not sure, read the appropriate sections before making your selection.

☒ Life sciences ☐ Behavioural & social sciences ☐ Ecological, evolutionary & environmental sciences

For a reference copy of the document with all sections, see nature.com/documents/nr-reporting-summary-flat.pdf

Life sciences study design

All studies must disclose on these points even when the disclosure is negative.

Sample size	No statistical sample size calculation was performed. Sample sizes were based on prior experience of suitable n numbers for ERG recordings in mice and a minimum of n of 3 animals for each condition (Vinberg et al. 2017, doi:10.7554/eLife.24550, Leinonen et al. 2020 eLife DOI: 10.7554/eLife.59422). CMP analyses sample size was a minimum of 3 animals for each condition based on prior experience (Marc et al. 1995, J Neurosci 15, 5106-5129). Human donor retina and macaque experiment sample sizes could not be predetermined and were based upon tissue and donor availability. We had 17 research donors, 3 donations after cardiac death, 5 donations after brain death, and 3 macaques included in this study.
Data exclusions	For human research donor maculae that did not respond, Rmax was set to 0 uV for analysis. When analyzing phototransduction parameters (e.g. time-to-peak and amplification constant) based on ex vivo ERG data, samples with Rmax < ~5uV were excluded due to low signal-to-noise-ratio. Two I1/2 outlier values from human retina samples (Supplementary Table 2) are reported but were excluded from mean calculations.
Replication	Retinal responses to different intensities of light were replicated by taking multiple responses from each retina to each light intensity measured while minimizing photoreceptor photopigment bleaching (minimum 3 repeats taken for the brightest intensity used, maximum of 10 for dim flash intensities). Responses from each retina replicated successfully and the average of these replicated responses was used for analyses. Each ex vivo ERG experiment was repeated in multiple animals (n numbers reported in figures, minimum of 3) across multiple different experimental days (between 6 - 11 days). IHC analyses was performed on multiple retinas (n >3) prepared on multiple days (2). Replication of results was successful for all mouse experiments. Almost every biological replicate in human experiments had a unique postmortem enculeation delay, i.e. we did not have biological replicates for every enucleation delay time point. For analysis of dominant times constant, kinetic and sensitivity parameters from organ donations after brain death we had at minimum of 2 biological replicates and minimum of 5 technical replicates (different tissue samples) for both macula and periphery.
Randomization	For analyses of pH and hypoxia effects an eye from each animal, of random sex, used was randomly allocated to the control or condition groups, the order each was recorded was alternated so that recording order was not a factor. For analyses of enucleation delay, each eye from each animal was allocated two time conditions randomly ranging between 0 min to 3h. For practical reasons the first eye recorded from each animal necessarily was assigned to the shorter enucleation delay.
Blinding	It was not possible to completely blind researchers to research donor enucleation delays since this information was provided by eye bank prior to acceptance of tissues. For experimental reasons it was not possible to blind investigators to postmortem delay time, pH or hypoxia condition or control groups during mouse ex and in vivo ERG experiments. However, investigators were blinded during analyses until summary statistics/condition group comparisons were carried out. For IHC and CMP acquisition and analyses investigators were blinded until summary statistics/condition group comparisons.

Reporting for specific materials, systems and methods

We require information from authors about some types of materials, experimental systems and methods used in many studies. Here, indicate whether each material, system or method listed is relevant to your study. If you are not sure if a list item applies to your research, read the appropriate section before selecting a response.

Materials & experimental systems

n/a	Involved in the study
☐	☒ Antibodies
☒	☐ Eukaryotic cell lines
☒	☐ Palaeontology and archaeology
☐	☒ Animals and other organisms
☒	☐ Human research participants
☒	☐ Clinical data
☒	☐ Dual use research of concern

Methods

n/a	Involved in the study
☒	☐ ChIP-seq
☒	☐ Flow cytometry
☒	☐ MRI-based neuroimaging

Antibodies

Antibodies used	Anti-L-glutamate IgG (cat. no. E100R), anti-taurine IgG (cat. no. TT100R), anti-L-glutamine IgG (cat. no. Q100R), anti-GABA IgG (cat. no. YY100R), anti-glycine IgG (cat. no. G100R), Anti-glutathione IgG (cat. no. J100R) , Anti-L-aspartate IgG (cat. no. D100R), Anti-L-

arginine IgG (cat. no. R100R) from Signature immunologics. Anti-CRALBP IgG (RRID: AB_2314227) gift from Dr. Jack Saar, anti-rod opsin 1d4 IgG (RRID: AB_2315015) Gift of Dr. Robert Molday. Anti-GFAP IgG (cat. no. Z0334) Dako. Anti-Cone red/green Opsin IgG (cat. no. AB5405) EMD Millipore . Anti activated caspase 3 (cat. no. 559565) from BD Pharmingen.

Validation

CMP antibodies Anti-L-glutamate IgG (cat. no. E100R), anti-taurine IgG (cat. no. TT100R), anti-L-glutamine IgG (cat. no. Q100R), anti-GABA IgG (cat. no. YY100R), anti-glycine IgG (cat. no. G100R), Anti-glutathione IgG (cat. no. J100R) , Anti-L-aspartate IgG (cat. no. D100R), Anti-L-arginine IgG (cat. no. R100R) from Signature immunologics:
All antihapten IgGs from Signature Immunologics (Table) have been extensively characterized in prior publications (Marc et al., 1995; Marc, 1999; Marc and Cameron, 2002; Marc and Jones, 2002). Each IgG is an isotype (determined by affinity chromatography and immunoblotting) that are produced in rabbit hosts immunized with glutaraldehyde–amino acid conjugates to bovine serum albumin (BSA) as described in Marc et al. (1995). Five separate analysis characterized the specificity and detectability of each anti-hapten IgG: 1) dependence on target molecule trapping with glutaraldehyde; 2) immunodot assays against the cognate of small molecule–proteins; 3) binding curves on quantitative artificial antigen stacks; and 4) cluster analysis (Marc et al., 1995).

CMP antibodies Anti-CRALBP IgG (RRID: AB_2314227) gift from Dr. Jack Saar, anti-rod opsin 1d4 IgG (RRID: AB_2315015) Gift of Dr. Robert Molday. Anti-GFAP IgG (cat. no. Z0334) Dako. Anti-Cone red/green Opsin IgG (cat. no. AB5405) EMD Millipore:

Anti activated caspase 3 (cat. no. 559565) from BD Pharmingen:
Tested in mouse and human cells by Western blot and flow cytometry by manufacturer.

Animals and other organisms

Policy information about studies involving animals; ARRIVE guidelines recommended for reporting animal research

Laboratory animals

C57Bl/6J males and females were obtained at >2 months from JAX laboratories. Gnat1-/- mice were bred in house on C57Bl6J background, males and females, >2 months. Mice were kept in standard housing with litter mates, provided with food and water ad libitum and maintained on a 12:12 (light-dark) cycle. Ambient temperature was maintained at 21 degrees celcius and humidity maintained at approximately 20%.

Wild animals

No wild animals were used in this study.

Field-collected samples

No field-collected sampled were used in this study.

Ethics oversight

Animal protocols were approved by the University of Utah Institutional Animal Care and Use Committee. All procedures related to human tissue procurement were carried out by representatives from the organ donor society Lifesharing, the Utah Lions Eye bank or the San Diego Eye bank, which are fully accredited for donor eligibility determination, recovery and distribution by the FDA, the Association of Organ Procurement Organizations (AOPO) and the Eye Bank of America Association. For these reasons, research was provided IRB exempt status by the University of Utah and Scripps Health (IRB #00106658 and #16-6781).

Note that full information on the approval of the study protocol must also be provided in the manuscript.